Flow enhanced non-linear magnetophoresis for high-resolution chip based bioseparation

Peng Li[†], *Aamer Mahmood* [‡], *and Gil U Lee*[†*]

[†]School of Chemistry and Chemical Biology, University College Dublin, Belfield, Dublin 4, Ireland
[‡]Birck Nanotechnology Centre, Purdue University, West Lafayette, IN 47906, USA
[*]To whom correspondence should be addressed. E-mail: gil.lee@ucd.ie
Authors email address: peng.li@ucd.ie, amahmood@purdue.edu, gil.lee@ucd

TITLE RUNNING HEAD Flow enhanced non-linear magnetophoresis for high-resolution bio-separation.

ABSTRACT. A new mode of magnetophoresis is described that was capable of separating superparamagnetic micro-beads from complex mixtures. Laminar flow and a rotating external magnetic field were applied to superparamagnetic beads assembled on a semi-periodic micro-magnets array. Beads at the edge of the micro-magnet array oscillated in-phase with amplitude that decreased with increasing rotation frequency of rotating magnetic field. Laminar flow along the edge of the array can be tuned to sweep the beads downstream at rotation frequency of external magnetic field lower than a threshold for corresponding beads. This threshold frequency depends on beads geometric and magnetic property. At the rotation frequency higher than the threshold frequency, the corresponding beads were immobilized on micro-magnets array and its edge thus the beads can no longer be swept by flow. Flow enhanced non-linear magnetophoresis (F-NLM) allowed superparamagnetic materials to be efficiently separated enabling efficient fractionation of multiple cells types and multiplexed diagnostic assays in which are attached or functionalized with different beads.

KEYWORDS Magnetic separation, magnetophoresis, superparamagnetic beads, micro-magnet arrays, diagnostic assays, cell separation, and lab-on-a-chip.

Our ability to understand and work with living systems is based on separation – bioseparation is the basis for determining the molecular state of a cell, or whole organism, and defines our capacity to utilize biologically derived molecules[1]. Currently, bioseparation is most often performed using liquid chromatography[2], electrophoresis[3] or centrifugation[4], which achieves separation by transporting an analyte relative to a stationary phase based on a physical or chemical property, such as surface chemistry, size, charge, or mass density. Although these techniques are able to separate analytes with a high resolution it is widely recognized that they are slow and often difficult to implement.

One approach to increasing the speed of separation was to use suspensions of micron-size superparamagnetic beads to perform magnetically activated separation[5, 6]. In this technique the beads are functionalized with a receptor against a specific analyte and reacted with a sample using chemical schemes similar to those developed for affinity chromatography. The beads are removed from the sample in a high-gradient magnetic field and can then be re-suspended after several washing steps due to their superparamagnetic properties. The increased speed of this technique results from rapid mass and fluid transport conditions produced by suspending the micro-beads in the sample. Superparamagnetic beads have proven to be well suited for lab-on-a-chip separation of rare cell types[7, 8] and highly sensitive bioanalytical measurements[9-13]. Current limitation of this technique are that separation is limited to a small number of analytes and can lead to aggregation of the magnetic beads on the cells, which complicates the recovery of viable rare cell types.

We have recently demonstrated non-linear magnetophoretic separation (NLM) of superparamagnetic beads on a micro-magnet array using an external, rotating magnetic field to create a translating, periodic magnetic field[14]. Beads exposed to this translating potential energy landscape moved across the micro-magnet array at a rate that was determined by the frequency of the external field rotation, ω, as well as the characteristic properties of the beads and array. At low frequencies, the magnetic beads became

locked in the potential energy landscape and travelled between adjacent magnets with a speed that was proportional to the velocity of the landscape. As the frequency was increased over a limit the beads can no longer remain in the local magnetic potential energy minima due to the force produced by hydrodynamic drag and became immobilized on a micro-magnet. The critical rotation frequency for a type of bead, which was defined as the frequency at which the average bead velocity started to diverge from the velocity of the translating potential energy landscape, has been introduced to characterize the transport behaviors of different beads at rotating magnetic field on micro-magnets array. The critical rotation frequency is dependent on the geometric and magnetic properties of the superparamagnetic beads and micro-magnets, for each type of bead. At critical frequency, the beads start to become immobilized on magnets array until they are completely immobilized on magnets array, as the rotation frequency increased. By applying separation frequencies, which higher than critical frequencies for a type of bead so all this type of bead can be immobilized on the magnets array while another type of bead, which has relative higher critical frequency for the beads are remaining transporting on magnets array, different superparamagneitc beads on micro-magnets array can be separated efficiently. NLM was used to isolate *B. globigii* and *S. cerevisiae* captured on 1.0 and 2.8 μm diameter magnetic beads by setting separation frequency at a value that higher than the critical frequency of complex, which composed of micro-beads and it attached microorganisms, but lower than critical frequency of bare micro-beads. Although NLM appears to overcome some of the limitations of linear magnetophoresis, the relatively small number of beads that can be manipulated on a single chip currently limits its wider application[14].

In this study we examined the influence of hydrodynamic flow on non-linear magnetophoresis of superparamagnetic micro-beads on the micro-magnets array. At low hydrodynamic velocities of flow, NLM transport, as described previously[14], remained unchanged on micro-magnet array. The beads became displaced from the array as the flow rate was increased to a limit. The transport behavior of the beads at constant flow rate was also studied on the edge of micro-magnets array, as shown in Figure 1.

In the absence of flow, the beads oscillated between a point on the edge of the micro-magnets and a point in the area adjacent to the array with amplitude, ΔX, which decreased with increasing frequency. At low rotation frequency of external magnetic field, the beads on the edge of magnet arrays were swept downstream along the edge (in *y*-direction) as the beads oscillating in *x*-direction. The velocity of beads along the edge of the array in *y*-direction was found to be strongly affected by rotation frequency of external magnetic field, i.e., the beads were trapped on the edge of the micro-magnets array and were unable to be swept by flow at rotation frequencies higher than a threshold, Ω_t, for conrresponding beads. The Ω_t for a type of bead was associated with geometric (size) and magnetic properties of the bead. As shown in Figure 1, at a rotation frequency which was higher than the threshold frequency for small beads but lower than that for large beads (i.e., the threshold frequency for smaller bead is relative lower than that for large bead in this case[14]), the large beads were swept along the edge of the micro-magnet array in the *y*-direction while the smaller beads remained trapped on the array. This study describes the transport of magnetic micro-beads on a semi-continuous micro-magnets array for different beads at presence of laminar flow as function of flow rate and external magnetic field rotation frequency.

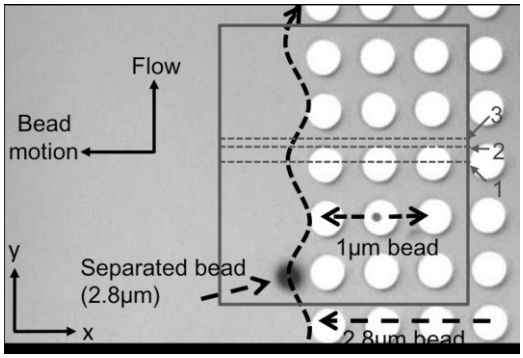

Figure 1. Top-veiw optical image of the micro-magnets array (white circles) on which 1.0 and 2.8 μm diameter superparamagnetic beads (black circles) are suspended. The micro-magnets have been magnetized in the *x*-direction, the external magnetic field is rotated around the *y*-axis, and a lanminar flow is produced in the *y*-direction. At 100 μl/min of flow rate, the motion of the beads under a 9 Hz rate of rotation of the external field has been drawn on the figure with dashed lines. The 2.8 μm beads

moved to the edge of the array and then moved along its edge in the flow. The 1.0 μm beads are trapped on the array. The gray rectangle delineates the region in which the finite element modelling (FEM) was preformed, which are described in the Discussion and Supplementary Mateirals. The dash lines indicated three cross-sections images presented in simulation figures.

Experimental

Microfabrication of the F-NLM flow chip with micro-magnets array The F-NLM chip was composed of an array of micro-magnets embedded in a flow chamber with fluidic ports. The regular photolithographic lift-off process was used to fabricate the cobalt micro-magnets with a high degree of dimensional control. The micro-magnet array was composed of 5 μm diameter circular magnets arranged in a square lattice with an 8 μm centre-to-centre distance. The cobalt micro-magnets were created by thermally depositing of 5 nm thick chromium, 70 nm thick cobalt, and 5 nm thick chromium sequentially on the patterned photoresist. After lift-off process, the micro-magnets arrays were subsequently coated with a 600 nm thick spin-on-glass (SOG) layer (Filmtronics, Butler, PA, USA) to provide chemical protection and regulate the magnetic field strength above the SOG surface. The flow chamber around the micro-magnets array was formed using a SU-8 (MicroChem, Newton, MA, USA) photolithographic process. The rectangular region of flow channel was 47 mm long, 7.8 mm wide, and 70 μm high. 170 μm thick glass cover sheet was bonded on top of SU-8 layer to form a closed chamber. Laser machining was used to drill 1mm diameter inlet and outlet holes in the substrate of micro-magnets chip. Customized and commercial NanoPort™ (Upchurch Scientific, Oak Harbor, WA, USA) micro-fluidic assemblies were used as the inter-connections to introduce samples and fluid in and out from precision syringe pumps and reservoirs. *The supplementary figure 1(a)* and *(b)* presented the photo of fabricated micro-magnets array and NLM chip.

External magnetic field and separation set-up A rotating magnetic field orthogonal to the axis of flow on the F-NLM chip was generated with three electromagnets[14]. The iron core solenoids have

diameter of 60 mm and length of 150 mm. Two synchronized sinusoidal signals with a 90-degree phase difference were generated with a two-channel function generator (Tektronix, Beaverton, Oregon, USA) with frequencies in range of 0.1 Hz to 100 Hz. The generated signals were amplified to the desired current using two programmable amplifiers (Kepco, Flushing, NY, USA) that was supplied to the electromagnets assembled in the *x* and *z*-axes. This generated an elliptical, rotating magnetic field with amplitude of 48 and 29 Gauss in the *x*-direction and *z*-directions, respectively. From the experiments, we observed that the beads motion behavior more stable in this elliptical rotating field. The rotation frequency of rotating magnetic field was precisely controlled by adjusting the frequency of these two synchronized sinusoidal signals.

In a typical separation experiment the samples were introduced into the flow chamber and then paused for one minute to allow the magnetic beads to be collected efficiently on the micro-magnets array with the *z*-direction electromagnet. Off-chip fluidic handling was used to control the flow on-chip and collect magnetic beads fractions. Precision syringe pumps (Chemyx, Stafford, TX, USA) were used to introduce sample and carrier fluids at specified flow-rates between 20 and 300 µl/min. The micro-PIV system was used to characterize the velocity of flow in flow chamber to obtain the precise velocity profile on the surface of flow chamber. F-NLM separation was executed after the beads were collected on the micro-magnet array by introducing carrier fluid into the chamber at a defined flow rate and activating the rotating magnetic field at specific rotation frequencies. Samples fractions separated at specific frequencies were collected using a valve manifold on the outlet port of the flow chamber. The schematic of separation system with NLM chip (with flow chamber), electromagnets, and fluidic handling was shown in *supplementary figure 1(c).*

The transport properties of beads in the F-NLM device were characterized with an epi-illumination, optical microscope (Zeiss Axioskop 2, Welwyn Garden City, UK) with a 63x long-working distance lens. Images of the magnetic beads on the micro-magnets array were acquired with a high-speed camera (Axiocam Hsm, Zeiss) with resolution of 660x494 pixels and at least 50fps. The velocities of

beads were analyzed by processing of recorded images sequences using time-lapse mode of imaging software, AxioVision (Carl Zeiss, Goettingen, Germany). At least 10 beads were measured in each experimental data point to obtain statistical results.

Reagents Two superparamagnetic beads were used in this study, i.e., carboxyl coated Dynabeads MyOne^{TM} and M-270^{TM} beads were purchased from Invitrogen (Carlsbad, CA, USA). The diameters of the beads were measured with scanning electron microscopy (S-4300 Hitachi, Krefeld, Germany) to be 1.0 and 2.8 μm, respectively; with coefficient of variation of the diameter was less than 3%. The magnetic susceptibility (χ) of the beads were measured with SQUID magnetometry (Quantum Design, San Diego, CA, USA) at room temperature being 0.3 and 0.17 for the 1.0 and 2.8 μm beads, respectively. The beads were suspended in 1 mM phosphate buffered saline solution with 0.5% Triton X-100 solution (PBST), which was also used as the carrier and rinse fluid.

Results

Transport behavior of the micro-beads on the inland region of micro-magnets array The motion of magnetic beads on the micro-magnets array was studied as a function bead radius, a, external magnetic field rotation frequency, ω, and flow rate, q, with an optical microscope. In the absence of flow the beads were observed to move across the micro-magnet arrays at low frequencies but became immobilized at a characteristic critical rotation frequency, as previously reported[14]. We measured the critical rotation frequencies for the beads in current NLM chip. The similar results compared with previous study[14] were obtained showing that the critical rotation frequency for 1.0 and 2.8 μm diameter beads was 4.5 and 9.0 Hz, respectively. The slight higher critical rotation frequencies for current system were contributed to thickness differences of SOG and cobalt properties variation caused in process. The immobilizing frequency, ω_i, for magnetic bead was defined as the rotation frequency of magnetic field for a type of magnetic bead, at which majority of this type of magnetic beads was immobilized on the micro-magnet array. In current study, the immobilizing frequency was found to be 5.5 and 12.0 Hz for

the 1.0 and 2.8 μm diameter beads, respectively. Due to the magnetization differences in given lot of beads[15], the beads shown different velocity of transport at low rotation frequencies. The threshold frequency introduced a minimum frequency for immobilizing majority of corresponding beads on micro-magnets array.

The behavior of the beads on the inland region of micro-magnets array was also studied as a function of flow rate. At a flow rate less than 140 μl/min, very little change in NLM transport behavior (compared with NLM transport in previous report in static liquid) could be observed. The magnetic beads will not be held in flow direction by micro-magnets as the flow rate increased to a high rate, because the increased hydrodynamic force in flow directon became dominant dramatically thus the beads will be swept downstream by this force. At flow rate of 160 and 140 μl/min, the 1.0 and 2.8 μm beads began to displace with flow from the micro-magnet array, respectively. For efficient separation, we limited the flow rate to 100 μl /min in separation experiments to ensure the beads, which travelled or immobilized on micro-magnets array, can be confined in *y* direction and only have *x* direction motion.

Transport behavior of the micro-beads on the edge of the micro-magnets array When the beads reached the edge of the micro-magnets array, they were observed to oscillate between the edge of the outer micro-magnets and a position in the flow channel (non-magnets channel). Figure 2(a) presented the measured amplitude of this oscillation, ΔX, as a function of ω at flow rate is zero, where ΔX was defined as the distance from the edge of micro-magnet to the centre of the bead at the maximum distance from the micro-magnet. From Figure 2(a) we observed that ΔX decreased as ω increased until it became zero as the bead stuck to the micro-magnet. The frequency at which ΔX became zero was 17.0 and 25.0 Hz for the 1.0 and 2.8 μm bead, respectively. Furthermore, relative smaller ΔX can be observed for smaller beads at same rotation frequencies.

Figure 2(b) presented the measured velocity, V_y, of the beads, which were swept by flow and moved along the edge of the micro-magnets array in flow direction, as the function of rotation frequency ω at a

flow rate of 100 μl/min. We observed that at low rotation frequencies, the beads travelled in *x* direction from inland regions of micro-magnets array to the edge of the array then can be swept by flow and moved with flow to downstream. The moving velocity of the swept beads on the edge of array, V_y, decreased as rotation frequency increased until the beads on the edge of array stop moving downstream and sticking on the edge of array, i.e. V_y became zero, at a threshold frequency, Ω_t. Ω_t was found to be 7.0 and 16.0 Hz for the 1.0 μm and 2.8 μm beads, respectively. We found that the threshold frequencies for each type of beads were higher than the immobilizing frequencies for corresponding beads as mentioned previously. It implied that the mojarity of corresponding beads were completely immobilized on inland region and edge of micro-magnets array at rotation frequency was higher than their threshold frequency.

Figure 2(c) presents the measurement of V_y as a function of flow rate at two different rotation frequencies of external magnetic field for two beads. These results shown that the motion of the beads down the edge of the micro-magnets array in flow direction was a non-linear function of ω and large beads moved faster than the small beads at a given flow rate. In fact, at rotation frequency was 9Hz, which was higher than threshold frequency for 1.0 μm beads, the beads were immobilized in flow direction, i.e. V_y was zero over the measured flow rate until they were displaced by increased dydrodynamic forces at flow rate was 160 μl/min.

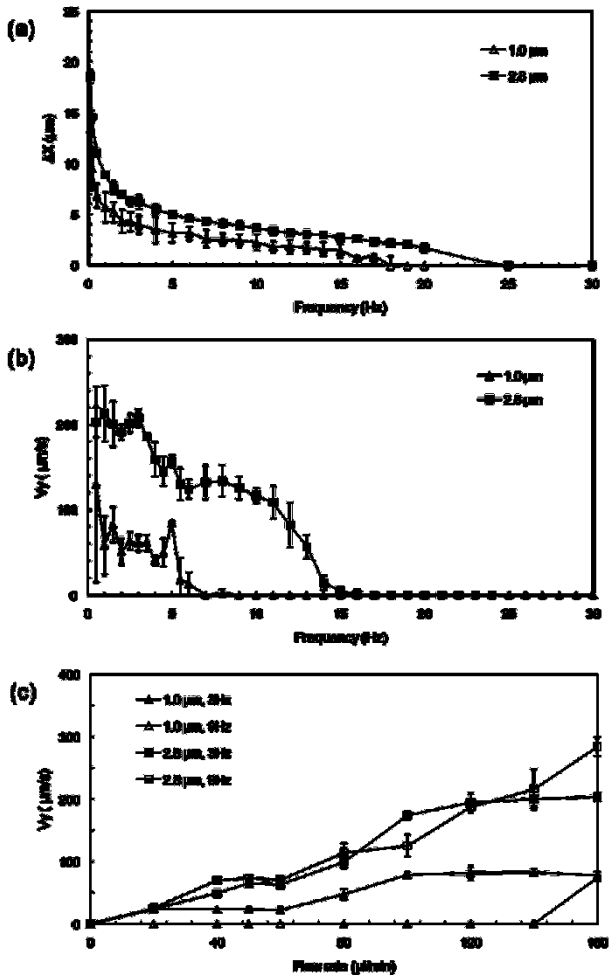

Figure 2. (a) Amplitude of oscilation of the beads, ΔX, on the edge of the micro-magnetic array as a fucntion of rotation frequency, ω, of exteranl magnetic field without flow. (b) Speed of bead motion in the direciton of flow at the edge of the micro-magent arrays, V_y, as a function of ω at q = 100 μl/min. The threshold frequency for two types of beads can be obtained at the V_y equal to zero. (c) V_y of 1.0 and 2.8 μm beads on the edge of the magnetic array as a function of q and ω. The data points shown the mean values and standard deviations (error bars) and each measurment was conducted at least ten beads for each data point in the data presented.

F-NLM separation of the magnetic micro-beads Separation of the magnetic beads using F-NLM was demonstrated by stepping ω through a series of frequencies at a flow rate of 100 μl/min. Figure 3 illutrated a three step separation process. Initially, the rotation frequency of external field was set at 30 Hz, which exceeded the immobilizing (ω_i) and threshold (Ω_t) frequencies for all two type beads. Figures

3(a), (b), and (c) show the beads at three time points and clearly illustrated that the beads fixed on the inland region and edge of the micro-magnet array. In second stage, the rotation frequency was decreased to 9 Hz where $\omega < \omega_{i,2.8\mu m} < \Omega_{t,2.8\mu m}$ and $\omega > \Omega_{t,1\mu m} > \omega_{i,1\mu m}$. Figures 3(d), (e), and (f) demonstrated that in this stage, the smaller 1.0 μm beads were fixed on the inland region and edge of micro-magnets array while the large beads moved across the array until they encounter the edge of array where they followed the direction of flow. In this way the larger beads were removed from the micro-magnets array while the 1.0 μm beads were trapped on the chip. In last step the frequency was decreased to 3Hz where $\omega < \omega_{i,1\mu m} < \Omega_{t,1\mu m}$. Figures 3(g), (h), and (i) illustrated that in this stage, the small beads were diplaced from the chip and separated in the laminar flow. This demonstration of F-NLM illustrated that it was capable of separating magnetic beads of different size and magnetization using the adjustable frequency of rotation of the external magnetic field. Any remaining beads on the array could be displaced by increasing the laminar flow to sweep them downstream.

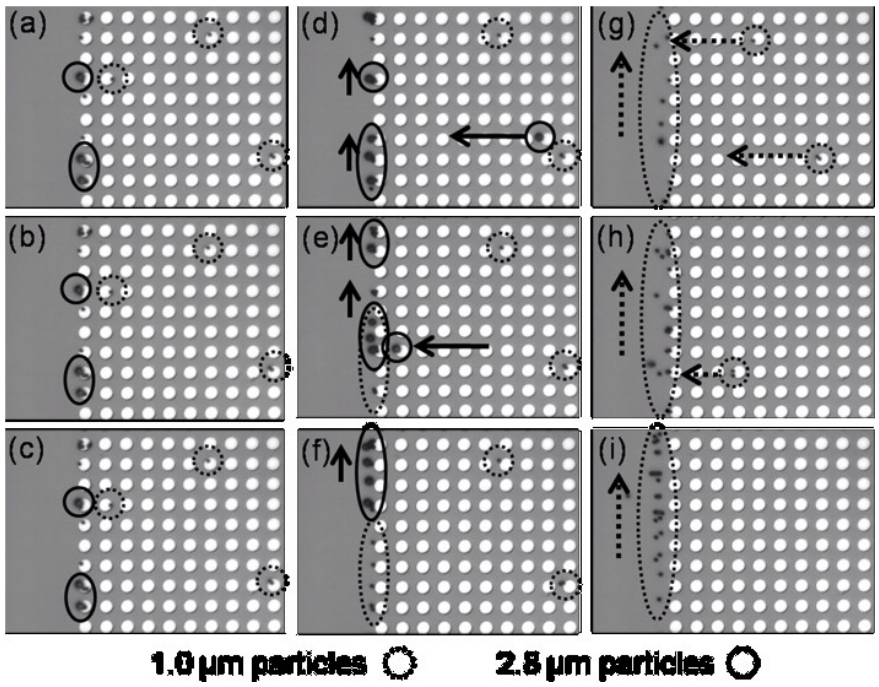

Figure 3. A sequence of screenshots of micrograph of showing the magnetic beads on the edge of micro-magnets array at different separation frequencies at q= 100 μm/min. Separation frequency was set to be 30 Hz in figure (a)-(c), 9 Hz in figure (d)-(f), and 3 Hz in figure (g)-(i).

Discussion

Analysis of motion of the beads on inland region of micro-magnets array The magnetic force applied to a superparamagnetic bead by a rotating magnetic field on a inland region of micro-magnets array has been previously described as

$$F_x(x,t) = F_{mag}\sin(kx - \omega t)\,, \qquad (1)$$

where F_{mag} is the maximum magnetic force acting on the bead on micro-magnets array and $k = \frac{2\pi}{d}$ is a constant describing the spatial periodicity of the micro-magnets array[14]. The solution of the equation of motion for this bead reveals the bead's motion can be described as an overdamped, non-linear oscillator. The critical frequency for a bead, which described previously, can be obtained by

$$\omega_c = \frac{\chi\mu_o\sigma_o H_{ext}}{18\eta}\left(2\pi\beta\right)^2\exp\left(-2\pi\beta\right) \qquad (2)$$

where μ_o is the permeability of free space, χ is susceptibility of magnetic bead, σ_o is an experimentally determined parameter representing the effective magnetic pole distribution on the array surface, H_{ext} is the magnitude of the external magnetic field, and β is the ratio of the bead radius, a, to the characteristic length scale of the array, d.

Overdamped, non-linear oscillators exhibit two distinct transport regimes depending on the rotation frequency of the external field. When the rotation frequency of external field was lower than the critical frequency for a type of bead, the bead reached a stable position within a given trap in the energy landscape and moved at a constant horizontal velocity with a speed equal to the translation velocity of the landscape, $\omega\frac{d}{2\pi}$. Near the critical frequency, the bead lagged behind the local energy minima. Above the critical frequency, the beads began to slip with respect to the translating potential energy landscape. Physically the slipping was observed as an oscillatory rocking motion between adjacent magnets

superimposed on a time-averaged linear velocity, which reduces to zero with increasing frequency at a rate defined by $\left(\omega - \sqrt{\omega^2 - \omega_c^2}\right)\frac{d}{2\pi}$.

Analysis of the motion of the beads at the edge of the micro-magnets array The magnetic field distribution at edge of a micro-magnets array was simulated using finite element modeling (FEM). Figure 4 presents cross-section view of the normal magnetic flux density, *B*, in *xz*-plane as the function of the angular degree of the external magnetic field to orientation of magnetization of micro-magnets, θ. The magnitude of *B* has been presented in false color with a single scale used for all eight images. Clearly, the *B* profiles do not have a simple functional form thus the equation of motion of a bead cannot be solved analytically for F-NLM. However, several of the key elements of the F-NLM behavior can be understood in terms of the magnetic potential energy, $U_m = -m \cdot B = -\frac{\chi \cdot V_m}{\mu_o} B^2$, and magnetic force applied to the magnetic beads, $F_m = (m\square \quad \cdot \chi \nabla \frac{B^2}{2\mu_o}$, where m is the dipole moment of the bead and V_m is the volume of the bead, as the magnetic bead trend to move to the region where the magnetic potential energy was the lowest, i.e. the region where the B was the highest in Figure 4.

The position of a magnetic bead on the edge of the array was drawn on Figure 4 at a point close to the highest local *B*, which represents the equilibrium position of the bead. Figure 4 provided insight into the motion of the magnetic beads at the edge of the micro-magnet array. It was seen that the *B* distribution surrounding the micro-magnets at the edge of the array had similar form to that on the inland region of array, particularly in the region adjacent the inland region. These *B* distributions allowed the beads to move from the inland region of array onto the outer micro-magnets as θ was rotated counter-clockwise from 0 to 360°. It also provided the driving magnetic force for the beads to enter the non-magnets flow channel and oscillate between a point on the edge of the outer micro-magnet and a point in the channel. From 0° to about 180°, the equilibrium position in the non-magnets flow channel moved outward until it reached the maximum amplitude at 180°. At meanwhile the magnetic force pushed the bead outward to follow this equilibrium position. Once the bead reached its maximum amplitude, the local equilibrium

position around bead started to move backward to micro-magnets array and the magnetic force pulled the bead to micro-magnets array, as magnetic field rotated from 180° to 315°, until the bead arrived onto the edge of micro-magnet at about 315°-0°. Then another cycle started and the bead will repeat above motion and formed a oscillation movement close to the edge of micro-magnets array.

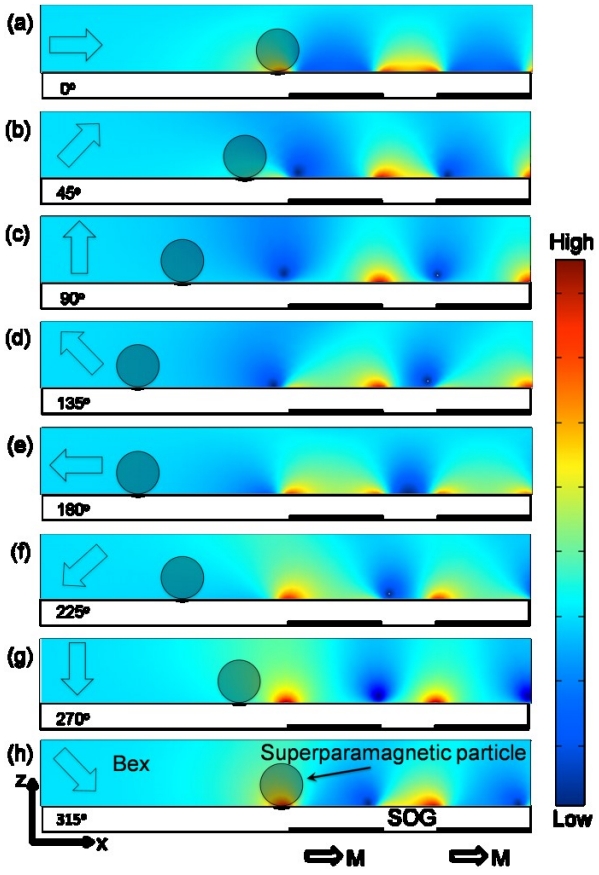

Figure 4. FEM simulated cross-section view of B distribution in an *xz*-plane through the centre of the micro-magnets presented as a function of angular degree between orientation of magnetization of micro-magnets and external magnetic field, θ. The magnitude of the external magnetic field, B_{ex}, was set to a value of 60 Gauss. The position of micro-magnets has been drawn as black bars at the bottom of each image. The thickness of cobalt micro-magnet and SOG layer was 70 nm and 600 nm, respectively. For simplicity, the surrounding materials were treated as nonmagnetic and the bead's inherent magnetization was not included in the simulation.

To analyze the quantitative positions of local equilibrium around the bead, as magnetic field rotating, the U_m in the center of a 1.0 μm bead at particular values of θ along the central-line of the two micro-magnets (Figure 1, Line 1) have been calculated based on FEM results, as shown in Figures 5(a) and (b). The lowest points in the curves in Figure 5(a) and 5(b) represented the U_m minimum where the bead trends to move into. These figures clearly supported the analysis obtained from the Figure 4. It clearly shown the magnetic bead was trapped in U_m minimum at the left edge of the outer micro-magnet and followed the movement of this U_m to reach the bead's maximum amplitude at θ was about 180°, as magnetic field rotating. From 180° to 315°, the bead has been pulled back to edge of micro-magnet then repeated the motion cycle at 0°. Because the high potential barrier on the position of edge of micro-magnets array at 0°, the bead cannot move back to inland of micro-magnet and repeat the new cycle again from 0°. The analysis explained the phenomenon of oscillation motion of bead observed on the edge of micro-magnets array in F-NLM as external magnetic field rotating at low rotation frequencies. Similar with the beads transport in NLM, as rotation frequency increased, the increased hydrodynamic forces drag the bead and the motion of the bead became "slipping" as presented previously in NLM system. Then the bead will be confined to the deepest U_m well, which corresponds the position of U_m at about 0°. This caused the decreasing of amplitude of bead on the edge of micro-magnets at high frequencies till the bead completely stucked on the edge of micro-magnets above threshold frequency.

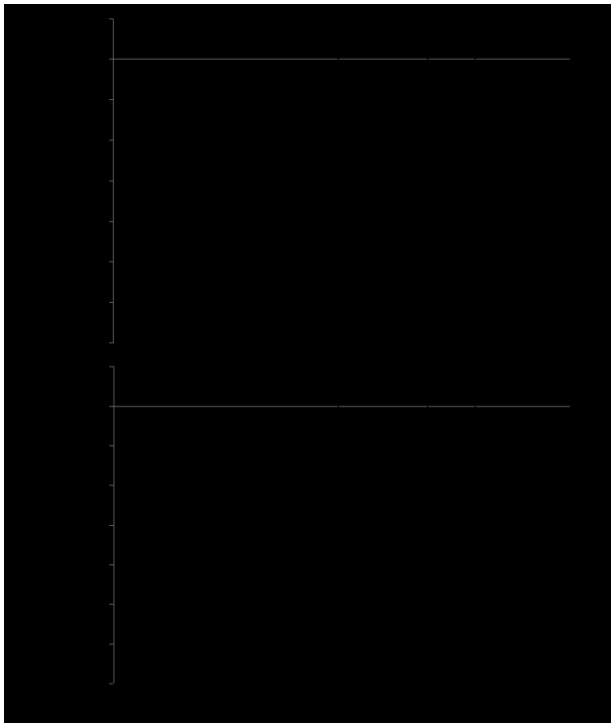

Figure 5. Magnetic potential energy at the edge of the micro-magnets array presented as a function of θ along Line 1 in Figure 1. Vertical dash lines have been used to identify the position of the micro-magnets as black bars in bottom presenting the micro-magnets. The magnetic bead was also illustrated as black dot in figure. (a). U_m for $0 < \theta < 180^o$. (b). U_m for $180 < \theta < 315^o$.

Three dimension FEM results of B distribution have been presented in the *Supplementary Section*. The FEM simulated the area enclosed by the rectangle in Figure 1 and the cross-section view of B distribution in the planes dissected by dash lines in Figure 1. All these figures clearly shown the similar forms with respect to the results shown in Figure 4. Thus, the beads experience dynamic magnetic flux densities and forces similar to those presented in Figure 4 as they moved to the edges micro-magnets array and started to oscillate on the edge at relative low rotation frequencies. As perpendicular flow applied, the resultant motion of bead caused by flow and oscillation of bead will be consistent with the motion of the beads illustrated in Figure 1 in which the beads moved along the edge of the micro-magnet array in a trajectory that varied in x.

F-NLM separation of the magnetic beads A movie of the F-NLM separation of the 1.0 and 2.8 μm beads was presented in the *Supplementary Section*. This movie demonstrated that at $\Omega_{t,1.0\ um} < \Omega_{t,2.8um} < \omega$ (30Hz), all types of beads on inland region of micro-magnets array and edges of micro-magnets array were immobilized. At $\Omega_{t,1.0\ um} < \omega$ (9Hz)$< \Omega_{t,2.8um}$,the 2.8 μm beads rapidly moved off and downstream from the edge of the micro-magnets array with flow. If the frequency was then shifted to ω (3Hz)$< \Omega_{t,1.0um}$, the remaining 1.0 μm beads rapidly moved off micro-magnets array and downstream with flow resulting in complete separation of these two beads populations.

This movie also highlighted the significant difference in V_y of the two beads populations as they move along the edge of the micro-magnetic array, due to the different magnitude of magnetic forces and hydrodynamic forces in *y* direction acted on these two beads. The hydrodynamic force experienced by a sphere in laminar flow at a surface can be calculated using Stokes equation, $F_h = -3\pi a v f_d$, where v is the fluid velocity at the center of the bead and the drag coefficient, $f_d = \left(1 + \frac{9}{16}\left(\frac{a}{h}\right)\right)$, is a function of bead radius, a, and height of the bead above the surface of the chamber, h[16]. The bead-substrate surface interaction was mediated by hydrodynamic lift forces, surface forces (which include Van der Waals attraction, electrostatic repulsion), and magnetic force in *z* component, which always pull the bead to the surface, due to superparamagnetic property of the magnetic bead. It was observed that the beads were confined on the surface of micro-magnets array in external rotating magnetic field over the all applied rotation frequencies, i.e. *h* was no more than 20% larger than *a.* The surface of SOG above micro-magnets array have been treated with surfactant to reduce the adhesion forces dramatically. This implied that the magnetic force in *z* component was dominant in these three forces. The resultant forces of these forces acted on beads, which suspended on micro-magnets array in rotating magnetic field, confined the beads on the surface and allowed the F-NLM separation can be implemented on surface.

To qualitatively understand the beads immobilizing behavior in *y* direction in the flow direction at rotation frequency higher than threshold frequency, we calculated the magnetic potential energy, U_m,

along the edge of array (in *y* direction) with different distance to the edge of array and *y*-component of the magnetic force, $F_{m,y}$, of a 1.0 μm bead along the edge of array with different distance to the edge. The results were shown in Figure 6. Figure 6(a) confirmed that the magnetic potential energy minimum, where the bead trend to move into, was located the center of micro-magnets at different distances. So, the bead has to be confined in these potential well and showing oscillation motion in rotating magnetic field, when there was on flow applied. When a flow applied, the hydrodynamic forces in *y* direction can possibly sweep the bead and break the potential barrier in *y* direction to move the bead downstream with flow, as long as the height of potential barrier was lower enough to allow hydrodynamic forces in *y* direction to breakthrough. It was clearly shown that the height of potential barrier increased dramatically as the distance to the edge decreased from 6 μm to 2 μm. When the beads average position was close to the edge of array, the potential barrier will increase to higher enough to overcome the hydrodynamic forces in *y* direction thus the bead will be confined in *y* direction by magnetic potential well unless the flow rate of flow increased correspondingly. From previous investigation we observed that as rotation frequency increased, the average distance from bead to edge of array decreased correspondingly, till the bead stuck on edge of array at frequencies above the threshold frequency. It was explained very well about the phenomenon we observed in F-NLM, i.e., the bead can be swept downstream with flow at low frequencies, but be immobilized on edge of array at rotation frequencies higher than threshold frequency. As mentioned before, due to immobilizing frequency typically lower than threshold frequency for same bead, the high efficient separation of beads can be implemented on micro-magnets array and edge of array. From Figure 6(b) the similar conclusion can be drawn that $F_{m,y}$ acted to center of the bead on the micro-magnet rapidly decreased in magnitude as *x* increased until it exceeded by hydrodynamic forces in y direction, thus allowing separation of bead in flow direction. Reflection on the motion of a bead at the edge of the micro-magnets array suggests that Ω_t was determined by the ΔX of the bead at which the restraining magnetic force, $F_{m,y}$, exceeds the hydrodynamic force in *y* direction. The hydrodynamic force applied to the 1.0 and 2.8 μm beads at

q=100 μl /min can be calculated to be 1.7 and 13 pN, respectively, if we assume h=0. Figure 6(b) suggests the hydrodynamic force is equivalent to magnetic force at $\Delta X \approx 2$ μm, which is in qualitative agreement with the observed behavior of the beads.

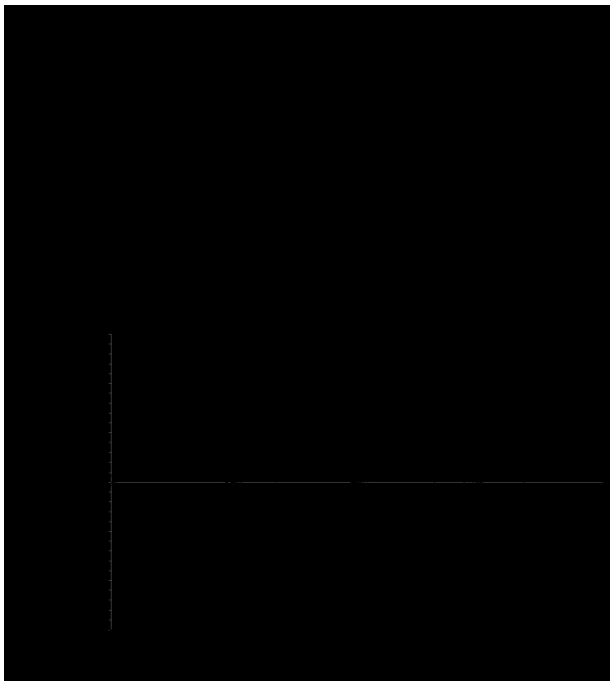

Figure 6. Magnetic potential energy (a) and force in the y-direction (b) experienced by a 1 μm bead in a line x μm away in front of the micro-magnets at the edge of the micro-magnets array for $\theta = 0^{o}$.The location of micro-magnets were indicated with black bars on bottom. In calculation the B fields were determined using 3D finite element analysis (*Supplementary Section*).

Conclusions

This manuscript described the transport behavior of superparamagnetic beads on a semi-continuous micro-magnet array in hydrodynamic flow field. Flow was observed to have a controlled influence on the motion of beads at the edge of a micro-magnetic array and the motion of the beads was observed to be a non-linear function of ω. Insight into this behavior was gained from finite element modeling of the magnetic flux density, B, at the edge of the array as a function of angular degree between external magnetic field and orientation of magnetization of micro-magnets, θ. As θ rotated from 0 to 360^{o} the

bead repeatedly travelled from the edge of the outer micro-magnet into the flow channel then back to the edge of the micro-magnet to follow the local U_m minimum. The high potential barriers on the inland side of micro-magnets stoped the bead moved back to inland region of micro-magnets array. It also provided a basis for understanding the physical mechanism for non-linear transport of the beads at the edge of the array with different rotation frequencies. The magnetic potential barrier and magnetic forces restrained the beads moving downstream with flow at the frequencies higher than threshold frequency, Ω_t. F-NLM appears to have a number of advantages as a separation technology over current magnetic separation technologies, i.e., it can be used to separate relatively high density of magnetic beads magnetic particles with a high degree of size and magnetization resolution with a in millilitre volumes. This leads us conclude that F-NLM promises to be highly use for sensing and cell separation applications where it should allow rapid separation of multiple analytes bound to superparamagnetic beads from milliliter volume samples.

Acknowledgement The authors acknowledge the Science Foundation of Ireland (Grants 08/RP1/B1376 and NAP158) and IRCSET for providing financial supporting for this work. We also thank Joe O'Brien and Mark Platt for helpful discussions.

References

(1) Baselt, D. R.; Lee, G. U.; Natesan, M.; Metzger, S. W.; Sheehan, P. E.; Colton, R. J. *Biosensors & Bioelectronics* **1998**, *13*, 731-739.
(2) Svedberg, T.; Fahraeus, R. *J Am Chem Soc* **1926**, *48*, 430-438.
(3) Tiselius, A. *T Faraday Soc* **1937**, *33*, 0524-0530.
(4) Tiselius, A.; Pedersen, K. O.; Svedberg, T. *Nature* **1937**, *140*, 848-849.
(5) Kemshead, J. T.; Gibson, F. J.; Ugelstad, J.; Rembaum, A. *P Am Assoc Canc Res* **1983**, *24*, 217-217.
(6) Kemshead, J. T.; Ugelstad, J.; Rembaum, A.; Gibson, F. *Eur J Cancer Clin On* **1982**, *18*, 1043-1043.
(7) Tibbe, A. G. J.; Grooth, B. G. d.; Greve, J.; Liberti, P. A.; Dolan, G. J.; Terstappen, L. W. M. M. *Nat Biotech* **1999**, *17*, 1210-1213.
(8) Han, K. H.; Frazier, A. B. *Lab Chip* **2006**, *6*, 265-273.
(9) Oh, B. K.; Park, S.; Millstone, J. E.; Lee, S. W.; Lee, K. B.; Mirkin, C. A. *J Am Chem Soc* **2006**, *128*, 11825-11829.

(10) Osterfeld, S. J.; Yu, H.; Gaster, R. S.; Caramuta, S.; Xu, L.; Han, S. J.; Hall, D. A.; Wilson, R. J.; Sun, S. H.; White, R. L.; Davis, R. W.; Pourmand, N.; Wang, S. X. *Porceedings of the National Academy of Sciences of teh United States of America* **2008**, *105*, 20637-20640.
(11) Bruls, D. M.; Evers, T. H.; Kahlman, J. A. H.; van Lankvelt, P. J. W.; Ovsyanko, M.; Pelssers, E. G. M.; Schielpen, J. J. H. B.; de Theije, F. K.; Verschurne, C. A.; van der Wijk, T.; van Zon, J. B. A.; Dittmer, W. U.; Immink, A. H. J.; Nieuwehnuis, J. H.; Prins, M. W. J. *LAB ON A CHIP* **2009**, *9*, 3504-3510.
(12) Godino, N.; Snakenborg, D.; Kutter, J. P.; Emmeus, J.; Hansen, M. F.; Munoz, F. X.; de. Campo, F. J. *Microfluidics and Nanofluidics* **2010**, *8*, 393-402.
(13) Gijs, M. A. M.; Lacharme, F.; Lehmann, U. *Chemical Reviews* **2010**, *110*, 1518-1563.
(14) Yellen, B. B.; Erb, R. M.; Son, H. S.; Hewlin, R.; Shang, H.; Lee, G. U. *Lab on a Chip* **2007**, *7*, 1681-1688.
(15) van Ommering, K.; Lamers, C. C. H.; Nieuwenhuis, J. H.; van Ijzendoorn, L. J.; Prins, M. W. J. *Journal of Applied Physics* **2009**, *105*, 10.

Supporting Information Available. Three supplementary figures and one movie

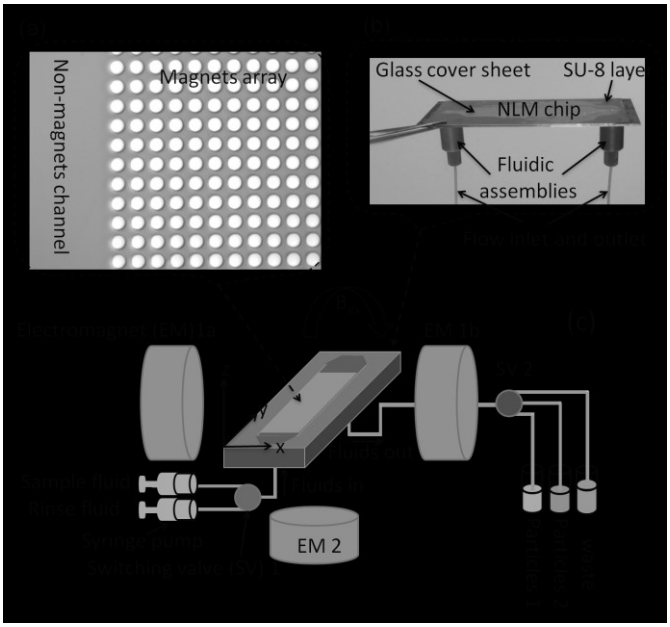

Supplementary Figure 1. Photos of microfabricated magnets array and NLM separator (a) and (b), and schematic of separation system set-up (c). (a) Microimges of cobalt micro-magnets array with 5 μm diameter circular micro-magnets and 8 μm center-to-center distance. The edge of magnets array was shown here as a non-magnets channel for separated beads moving downstream with flow. (b) Photo of fabricated NLM chip with magnets array enclosed by SU-8 flow chamber and glass cover sheet.

Microfluidic assemblies used for interconnections between flow chamber and off-chip fluidic handling. (c) Schematic of separation system set-up with NLM chip, electromagnets, and fluidic handling.

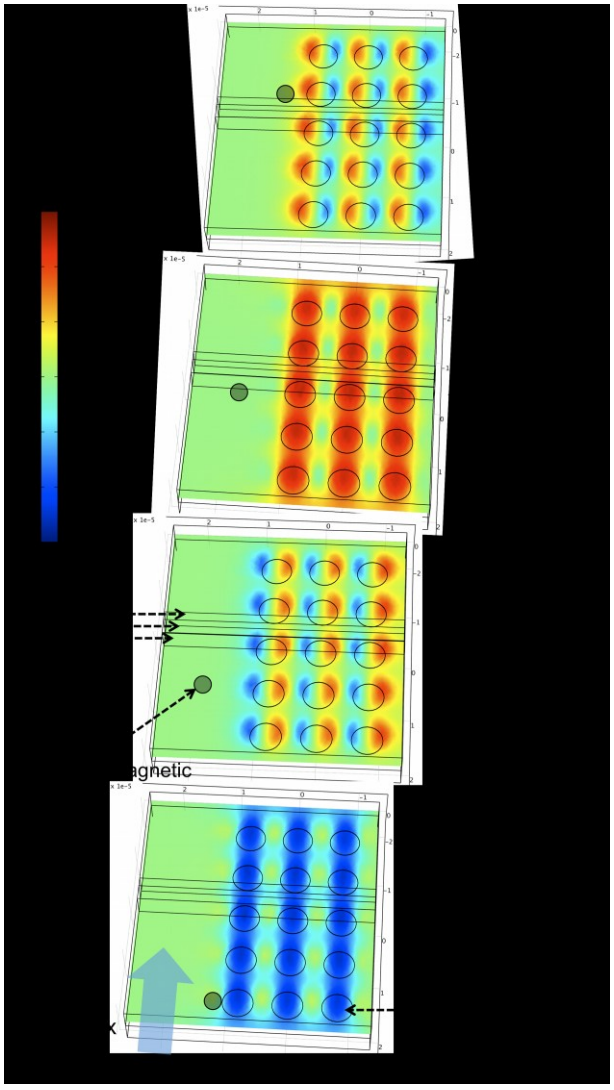

Supplementary Figure 2. Finite element simulation of the magnetic flux density in the *xy*-plane in the center of 2.8 μm bead, as angular degree between external magnetic field and the orientations of

magnetization of micro-magnets. The magnetic beads have been drawn in the region of local maximum magnetic flux density. The dash arrows indicated the planes which have beeen dissected to show cross-section view of finite element modelling were performed (results are shown in supplementary Figure 3).

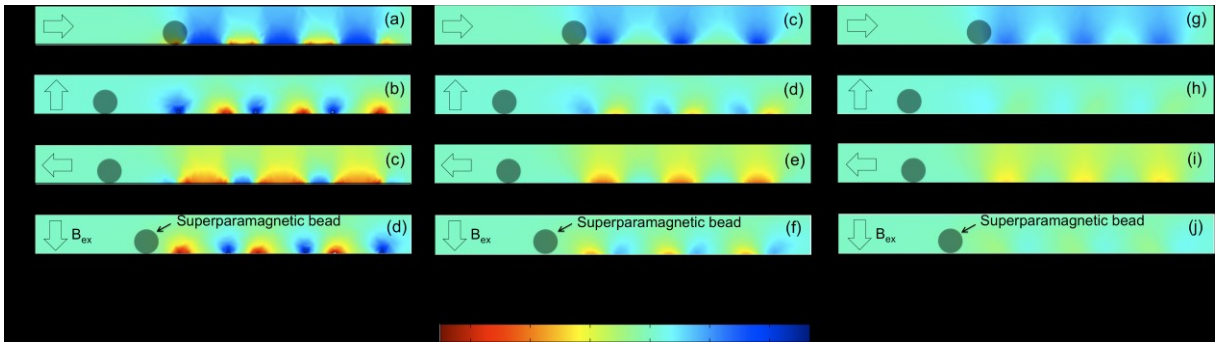

Supplementary Figure 3. Finite element simulation of the magnetic flux density in the *xz*-plane through the defined lines in Figure 1 in main context (defined planes in supplementary Figure 2) as angular degree between external magnetic field and the orientations of magnetization of micro-magnets. The magnetic beads have been drawn in the region of local maximum magnetic flux density. Figure (a) – (d) shown the results in plane defined by Line 1 (plane 1); Figure (e) – (df) shown the results in plane defined by Line 2 (plane 2); Figure (g) – (j) shown the results in plane defined by Line 3 (plane 3).